

ACOUSTIC RESONANCE BETWEEN GROUND AND THERMOSPHERE

Matsumura, M.,^{1*} Iyemori, T.,¹ Tanaka, Y.,² Han, D.,³ Nose, M.,¹ Utsugi, M.,¹ Oshiman, N.,⁴ Shinagawa, H.,⁵ Odagi, Y.¹ and Tabata, Y.⁶

¹Graduate School of Science, Kyoto University, Kyoto 606-8502, Japan

E-mail: mitsuru@kugi.kyoto-u.ac.jp

²Faculty of Engineering, Setsunan University, Neyagawa 572-8508, Japan

³Polar Research Institute of China, Pudong, Jinqiao Road 451, Shanghai 200136, China

⁴Disaster Prevention Research Institute, Kyoto University, Uji 611-0011, Japan

⁵National Institute of Information and Communications Technology, Koganei 184-8795, Japan

⁶Research Institute for Sustainable Humanosphere, Kyoto University, Uji 611-0011, Japan

ABSTRACT

Ultra-low frequency acoustic waves called "acoustic gravity waves" or "infrasounds" are theoretically expected to resonate between the ground and the thermosphere. This resonance is a very important phenomenon causing the coupling of the solid Earth, neutral atmosphere, and ionospheric plasma. This acoustic resonance, however, has not been confirmed by direct observations. In this study, atmospheric perturbations on the ground and ionospheric disturbances were observed and compared with each other to confirm the existence of resonance. Atmospheric perturbations were observed with a barometer, and ionospheric disturbances were observed using the HF Doppler method. An end point of resonance is in the ionosphere, where conductivity is high and the dynamo effect occurs. Thus, geomagnetic observation is also useful, so the geomagnetic data were compared with other data. Power spectral density was calculated and averaged for each month. Peaks appeared at the theoretically expected resonance frequencies in the pressure and HF Doppler data. The frequencies of the peaks varied with the seasons. This is probably because the vertical temperature profile of the atmosphere varies with the seasons, as does the reflection height of infrasounds. These results indicate that acoustic resonance occurs frequently.

Keywords: infrasound, acoustic resonance

1 INTRODUCTION

Acoustic waves are generated by various phenomena, for example, earthquakes, volcanic eruptions, thunderstorms, and typhoons. Ultra-low frequency acoustic waves are called "infrasounds". They are theoretically expected to resonate between the ground and the thermosphere, and through this resonance, affect the ionosphere and even the solid Earth.

In this section, the phenomena following the resonance are introduced, as is the mechanism of acoustic resonance.

1.1 Phenomena following acoustic resonance

1.1.1 Ionospheric disturbances

Even a small atmospheric perturbation near the Earth's surface results in a considerably large displacement at thermospheric heights. At around an altitude of 100 km, the collision frequency between ions and neutral particles is greater than gyrofrequency, so kinetic energy of the neutral atmosphere is transformed to that of plasma.

Vertical motions of ionospheric plasma can be observed as Doppler shifts of radio waves reflected at the ionosphere. A

transmitted radio wave is reflected at a height where the frequency of the wave is equal to that of the electron plasma. In the daytime, the pseudo reflection height is in the E region (about 100 km) for 5-MHz transmission waves and in the F region (about 300 km) for 8-MHz waves.

The relation between a Doppler shift Δf and vertical plasma speed v is

$$v = -\frac{\Delta f}{2f} \frac{c}{\cos \theta}, \quad (1)$$

where f is the carrier frequency, c is the speed of light in a vacuum, and θ is the angle of incidence of the sounding wave on the ionosphere [Artru et al., 2004].

By the above method, ionospheric disturbances have been observed in severe weather [Plasad et al., 1975; Davies and Jones, 1971]. In both studies, ionospheric disturbances of about 4-mHz frequency were dominant.

1.1.2 Geomagnetic pulsations

Through ionospheric disturbances, the kinetic energy of plasma can be transformed to electromagnetic energy, i.e., the dynamo effect can occur and the resulting dynamo current generates a magnetic field.

At the Sumatra earthquake 2004, a geomagnetic pulsation was observed [Iyemori et al., 2005]. In general, geomagnetic pulsations are considered to be caused by magnetospheric processes. However, the localized nature and the period (frequency) of the oscillations suggest that the pulsation was generated by dynamo action in the ionosphere, which was caused by the acoustic resonance set up by the earthquake. A spectral analysis showed the dominant frequency of the magnetic oscillation was 4.6 mHz. The vertical wind velocity 120km above the epicenter simulated by Shinagawa [2007] followed this mechanism. That simulation showed that the dominant frequency of the vertical oscillation generated by the earthquake was about 4 mHz.

1.1.3 Earth's background free oscillations

Another phenomenon connected to acoustic resonance is Earth's background free oscillations. Solid earth is always oscillating in specific modes, even without large seismic events. Acoustic resonance may be the source of the free oscillation. The amplitude of ${}_0S_{29}$, the dominant mode of the free oscillations, is enhanced every August [Nishida et al, 2000].

One interpretation of this phenomenon is as follows. The eigen frequency of ${}_0S_{29}$ is constant throughout the year, but that of ${}_0P_{29}$, an atmospheric resonance mode, varies annually in accordance with the variation of the atmospheric temperature profile. The eigen frequency of ${}_0P_{29}$ most closely approaches ${}_0S_{29}$ in August, enhancing the amplitude of ${}_0S_{29}$ [Nishida, 2000]. Annual variation of the eigen frequency of ${}_0S_{29}$ was proved through numerical calculation by Kobayashi [2007].

1.2 Mechanism

1.2.1 Acoustic resonance

Assuming that the atmosphere is compressible and density-stratified, the equations for conservation of mass, momentum, and energy are given by

$$\frac{\partial \rho}{\partial t} + \nabla \cdot (\rho \mathbf{u}) = 0, \quad (2)$$

$$\rho \left\{ \frac{\partial \mathbf{u}}{\partial t} + (\mathbf{u} \cdot \nabla) \mathbf{u} \right\} = -\nabla p + \rho \mathbf{g}, \quad (3)$$

$$\frac{\partial p}{\partial t} + (\mathbf{u} \cdot \nabla) p - \frac{\gamma p}{\rho} \left\{ \frac{\partial \rho}{\partial t} + (\mathbf{u} \cdot \nabla) \rho \right\} = 0, \quad (4)$$

respectively. The pressure p and density ρ are written as $p = p_0 + p_1$ and $\rho = \rho_0 + \rho_1$, where p_0 and ρ_0 represent the background states and p_1 and ρ_1 the perturbations from the background states.

We consider a two-dimensional wave propagation on the x - z plane. The above equations are then linearized as follows.

$$\frac{\partial}{\partial t} \left(\frac{\rho_1}{\rho_0} \right) - \frac{w}{H_\rho} + \frac{\partial u}{\partial x} + \frac{\partial w}{\partial z} = 0, \quad (5)$$

$$\frac{\partial u}{\partial t} = -\frac{c^2}{\gamma} \frac{\partial}{\partial x} \left(\frac{p_1}{p_0} \right), \quad (6)$$

$$\frac{\partial w}{\partial t} = -\frac{c^2}{\gamma} \frac{\partial}{\partial z} \left(\frac{p_1}{p_0} \right) + \left(\frac{p_1}{p_0} - \frac{\rho_1}{\rho_0} \right) g, \quad (7)$$

$$\frac{\partial}{\partial t} \left(\frac{p_1}{p_0} \right) - \frac{\gamma}{c^2} g w - \gamma \left\{ \frac{\partial}{\partial t} \left(\frac{\rho_1}{\rho_0} \right) - \frac{w}{H_\rho} \right\} = 0. \quad (8)$$

The scale height of mass density H_ρ and that of pressure H_p are defined as

$$\frac{1}{H_\rho} = -\frac{1}{\rho_0} \frac{\partial \rho_0}{\partial z}, \quad (9)$$

$$\frac{1}{H_p} = -\frac{1}{p_0} \frac{\partial p_0}{\partial z}, \quad (10)$$

respectively. From the equations of state and hydrostatic equilibrium, the scale height of pressure H_p becomes

$$H_p = \frac{RT_0}{g} = \frac{c^2}{\gamma g}. \quad (11)$$

The sound speed c is given by

$$c^2 = \frac{\gamma p_0}{\rho_0} = \gamma RT_0. \quad (12)$$

For plane waves, assuming the dependence of u , w , p_1/p_0 , and ρ_1/ρ_0 on x , z , and t in the form

$$\exp\{i(\omega t - kx - mz)\}$$

and substituting this in the linearized equations, we obtain

$$m_R^2 - \left(m_I - \frac{1}{2H_p} \right)^2 = \left(1 - \frac{\omega_a^2}{\omega^2} \right) \frac{\omega^2}{c^2} - k^2 \left(1 - \frac{\omega_b^2}{\omega^2} \right), \quad (13)$$

$$m_R \left(2m_I - \frac{1}{H_p} \right) = 0, \quad (14)$$

where

$$m = m_R + im_I. \quad (15)$$

$$\omega_a = \frac{c}{2H_p} \sqrt{1 + \frac{4}{\gamma} \left(\frac{H_p}{H_\rho} - 1 \right)}, \quad (16)$$

$$\omega_b = \frac{c}{\gamma H_p} \sqrt{\gamma \frac{H_p}{H_\rho} - 1}. \quad (17)$$

The angular frequencies ω_a and ω_b are the acoustic cutoff and the Brunt-Väisälä frequencies, respectively. From Eq. (14),

$$m_R = 0 \quad (18)$$

$$\text{or} \quad m_I = \frac{1}{2H_p}. \quad (19)$$

If $m_R \neq 0$, the phase of a wave shows that it can propagate in the vertical direction. In this case, using Eq. (19), we obtain

a dispersion relation described as

$$m_R^2 = \left(1 - \frac{\omega_a^2}{\omega^2}\right) \frac{\omega^2}{c^2} - k^2 \left(1 - \frac{\omega_b^2}{\omega^2}\right). \quad (20)$$

To satisfy $m_R \neq 0$, the right hand side of Eq. (20) must be greater than or equal to 0. From this condition, we obtain the ω - k diagram shown in Fig. 1. Waves in the upper shaded area are acoustic waves, and those in the lower shaded area are gravity waves. This figure shows that gravity waves cannot propagate in a purely vertical direction but acoustic waves can.

Now we consider a plane wave propagating vertically along the z axis, i.e., $k = 0$. Then, if the atmospheric perturbation is excited by a horizontal planar pressure source $p_s \exp(i\omega t)$ at $z = 0$, we obtain vertical velocity

$$w = \frac{\omega}{\gamma X} \frac{p_s}{p_0(z=0)} \exp(m_1 z) \exp\{i(\omega t - m_R z - \alpha)\}, \quad (21)$$

where

$$X = \sqrt{m_R^2 + \left(m_1 - \frac{1}{\gamma H_p}\right)^2}, \quad (22)$$

$$\cos \alpha = \frac{m_R}{X}, \quad \sin \alpha = \frac{1}{X} \left(m_1 - \frac{1}{\gamma H_p}\right). \quad (23)$$

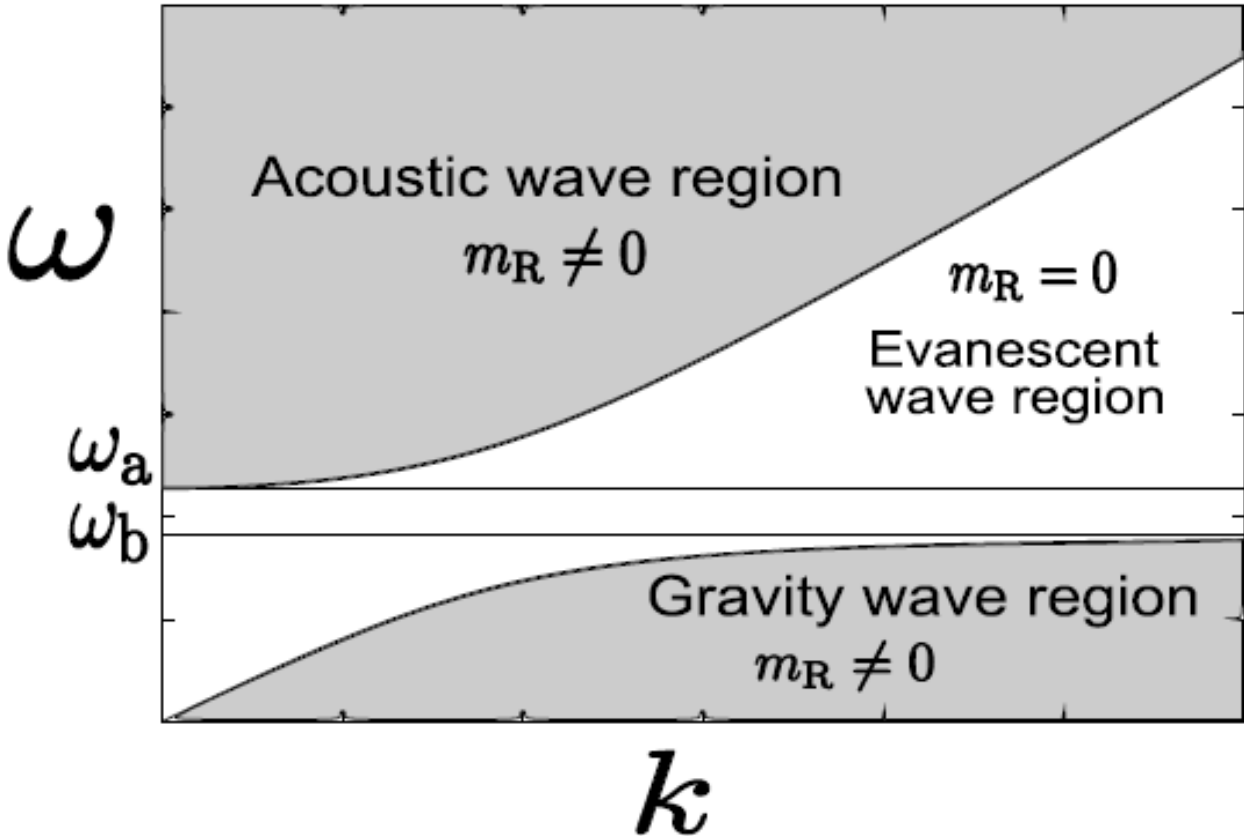


Figure 1: Dispersion diagram.

If $m_R \neq 0$ ($\omega > \omega_a$), from Eqs. (19) and (20),

$$w = \frac{\omega}{\gamma X} \frac{p_s}{p_0(z=0)} \exp\left(\frac{z}{2H_p}\right) \exp\left\{i\left(\omega t - \frac{\sqrt{\omega^2 - \omega_a^2}}{c} z - \alpha\right)\right\}. \quad (24)$$

The term $\exp(z/H_p)$ comes from the exponential decrease of density with altitude (Fig. 2) because the energy density is

proportional to $\rho_0 w^2$ and is conserved. This shows that even a small atmospheric perturbation near the surface results in a considerably large displacement at thermospheric heights. From Eq. (24), vertical perturbation with 1-Pa amplitude on the ground leads to vertical wind with amplitudes of tens of meters per second at an altitude of about 120 km.

The vertical phase and group speeds of an infrasound are

$$v_{ph,z} = \frac{\omega}{\sqrt{\omega^2 - \omega_a^2}} c, \tag{25}$$

$$v_{g,z} = \frac{\partial \omega}{\partial m_R} = \frac{m_R c}{\omega} = \frac{c}{v_{ph,z}},$$

respectively. The acoustic cutoff (angular) frequency ω_a varies with altitude, as shown in Fig. 2, because ω_a depends on temperature and temperature varies with altitude, as shown in Fig. 3. Atmospheric parameters are calculated with the MSIS-E-90 Model [Labitzka et al., 1985; Hedin, 1991] here.

A notable feature is that infrasounds of around 4-mHz frequency cannot propagate above a 100-km altitude.

For an infrasound of around 4-mHz frequency, ω_a at an altitude can be equal to ω , a frequency of the wave. Then, m_R becomes 0 and the propagation of the wave stops, the vertical phase speed (and wave length) diverges to infinity, and the group speed becomes 0 and the energy flow also stops.

In Eq. (16), c/H_p is dominant, showing that an acoustic cutoff is a frequency of the spatial pressure variation that acoustic waves experience. To be an acoustic wave, the gas must be compressed and expand more frequently than the pressure varies spatially. When the background temperature of the atmosphere decreases, the scale height of the pressure decreases and the spatial variation of the pressure is frequent. Therefore, an ultra-low frequency acoustic wave cannot exist as an acoustic wave at an altitude.

A part of the energy stopped at the cutoff altitude may leak through the evanescent region, but the other part is reflected back to the ground. Therefore, infrasounds can resonate between the ground and thermosphere.

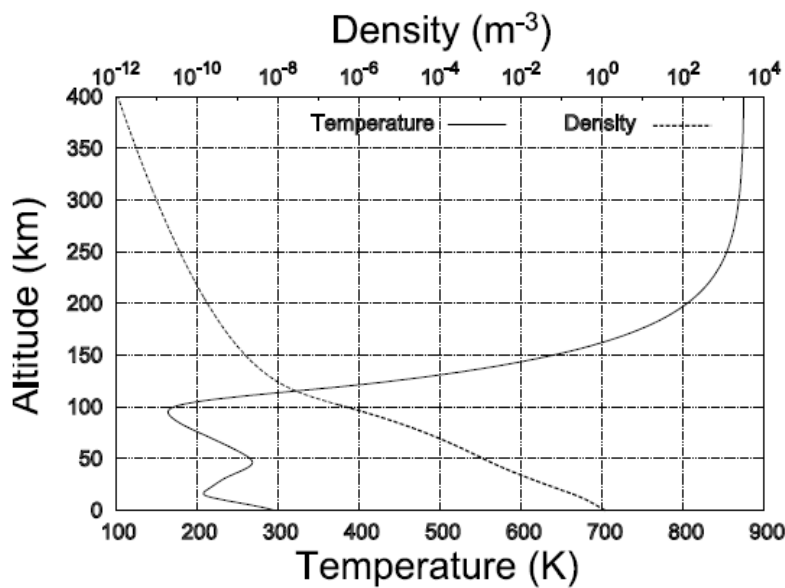


Figure 2: Temperature and density as function of altitude at 16:00 LT on June 23, 2007.

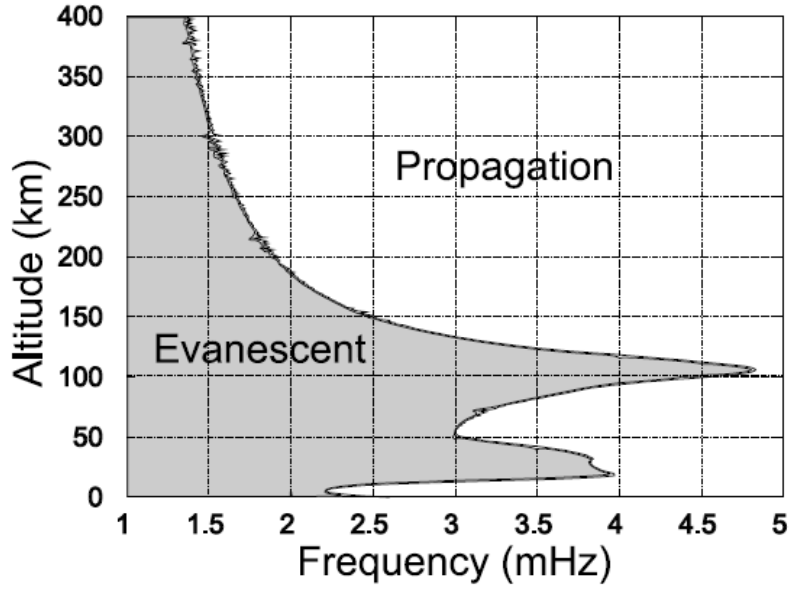


Figure 3: Acoustic cutoff frequency as function of altitude at 16:00 LT on June 23, 2007.

If $m_R = 0 (\omega \leq \omega_a)$, i.e., m is purely imaginary, waves cannot propagate in the vertical direction. In this case, we obtain m_1 from Eq. (13).

$$m_1 = \frac{1}{2H_p} \pm \sqrt{\left(\frac{\omega_a^2}{\omega^2} - 1\right) \frac{\omega^2}{c^2} + k^2 \left(1 - \frac{\omega_b^2}{\omega^2}\right)} \quad (26)$$

$$w = \frac{i\omega}{\gamma X} \frac{p_s}{p_0(z=0)} \exp\left\{\left(\frac{1}{2H_p} \pm \sqrt{\omega_a^2 - \omega^2}\right)z\right\} \exp\{i\omega t\}. \quad (27)$$

The condition of resonance is

$$\int_0^{h_{ref}} m_R dz = \frac{n\pi}{2}, \quad (28)$$

where n is an integer and h_{ref} is an altitude where $\omega = \omega_a$ and the wave is reflected. The frequencies of waves that satisfy this condition are 3.44, 3.88, 4.20, and 4.61 mHz for the atmosphere at 16:00 LT on June 23, 2007. These values are similar to those of other theoretical reports [Jones and Georges, 1976; Kobayashi, 2007; Lognonne et al., 1998; Nishida, 2000; Tahira, 1995]. The reflection heights corresponding to these frequencies are 80, 91, 97, and 101 km.

Eigen frequencies of higher modes are not equal to whole number multiples of the fundamental frequency because the reflection height depends on the frequency of the wave and as does how the vertical phase velocity varies. These eigen frequencies vary with time, day, month, year, and latitude because atmospheric parameters such as temperature and acoustic atmospheric cutoff frequencies change with these parameters.

1.2.2 Geomagnetic variations generated by infrasound

As described in the previous section, the reflection height of a resonance wave is about 100 km for higher modes, where the conductivity is high and the dynamo effect can occur.

Because the collision frequency between ionized particles and neutral particles is high in this region, ionized particles, especially positive ions, are dragged by neutral particles and move with them. The motion of these ions creates an electric field and generates electric current as follows:

$$j = \sigma V \times B, \quad (29)$$

where σ is the conductivity tensor and B is the background geomagnetic field. Then, geomagnetic variations are generated by the current.

1.2 Purpose of this study

Acoustic resonance is a very important phenomenon for understanding the coupling processes among solid earth, neutral atmosphere, and ionospheric plasma. Resonance itself, however, has not been directly confirmed with atmospheric pressure observations.

If acoustic resonance is confirmed to exist, thermospheric parameters may be estimated from observations on the ground considering the characteristics of acoustic resonance.

The main purpose of this study is to confirm the existence of resonance. To do this, observations of atmosphere on the ground and at the thermospheric heights are necessary. Thus, observation data of pressure perturbation on the ground and of ionospheric disturbance using HF Doppler shifts were used in this study. In addition, geomagnetic data were used because the reflection height of a resonance wave is close to the dynamo region, and geomagnetic variation may be useful for detecting or identifying acoustic resonance.

2 OBSERVATIONS AND ANALYSES

2.1 Statistical analyses

2.1.1 Data sets

With interest triggered by the magnetic pulsation event during the 2004 Sumatra earthquake, we have observed atmospheric pressure since the summer of 2006 at Shigaraki (34.8°N, 136.1°E). The barometric sensor resolution is about 1.6 Pa, and the output signal is A/D converted with 490-Hz sampling and 0.4-Pa resolution. One-second averaged data are recorded.

For comparison with the barometric observations, HF Doppler (HFD) data were used. The HF radio transmission site is at Chofu (34.7°N, 139.5°E). The HFD data was provided by Sugadaira Space Radio Observatory, University of Electro-Communication. There are several reception sites in Japan, and the Oarai site (36.3°N, 140.6°E) was used in our study. The elevation angle to the reflection point is 58.6° for 100 km and 78.2° for 300 km heights. The midpoint between the transmission and the reception site is at 36.0°N, 140.1°E. The frequency of the transmission wave used in this study was 5.006 MHz. The reflection height of radio waves at this frequency is about 100 km, the E region of the ionosphere, which is close to the theoretically expected reflection height of the resonance wave. These data were sampled once every 10 s.

One-second sampled data from a fluxgate magnetometer at Aso (32.9°N, 131°E) were also used. The resolution of the magnetometer was 0.1 nT. If acoustic resonance is the source of the Earth's background free oscillations, the acoustic resonance must occur frequently. Therefore, statistical analyses will be useful to confirm the existence of acoustic resonance.

The data from September 2006 to December 2008 were analyzed, although the pressure data after August 2008, HFD data for December 2007, and magnetic components data from September 27 to December 11, 2007 were missing.

2.1.2 Mean power spectral densities over 12 months

Barometric data were compared with HFD and magnetic data. The mean power spectral densities (PSDs) for every month in 2007 are shown in Fig. 4. The data for six hours were used to calculate each PSD, and PSDs thus calculated were averaged for a day and a month in the logarithmic scale. For HFD, however, PSDs were not averaged for a day and the data from 09:00 to 15:00 LT were used because the density of ionospheric plasma decreases at night and the reflection heights of HF radio waves are quite different from daytime ones. For HFD, "Lag" was set to 139, i.e., 1390 s, about $3(\text{datalength})^{1/2}$, following Hino (1977). "Lag" for the pressure and magnetic components was the same, although the data length was 10 times that of HFD.

As for pressure, peaks appeared between 3 and 4 mHz, which was especially clear in April to October. The frequencies of the peaks varied with the months. For HFD, there were peaks at 3–5 mHz for almost all the months. For the magnetic H component, small peaks around 6 mHz were seen in January to May, and for the D component, peaks around 4.5 and 5.5 mHz were seen in January to June. For HFD and the magnetic components, the spectra in the case of geomagnetic ap index ≤ 9 were used to decrease the effects of ionospheric disturbances and geomagnetic pulsations caused by magnetospheric plasma processes.

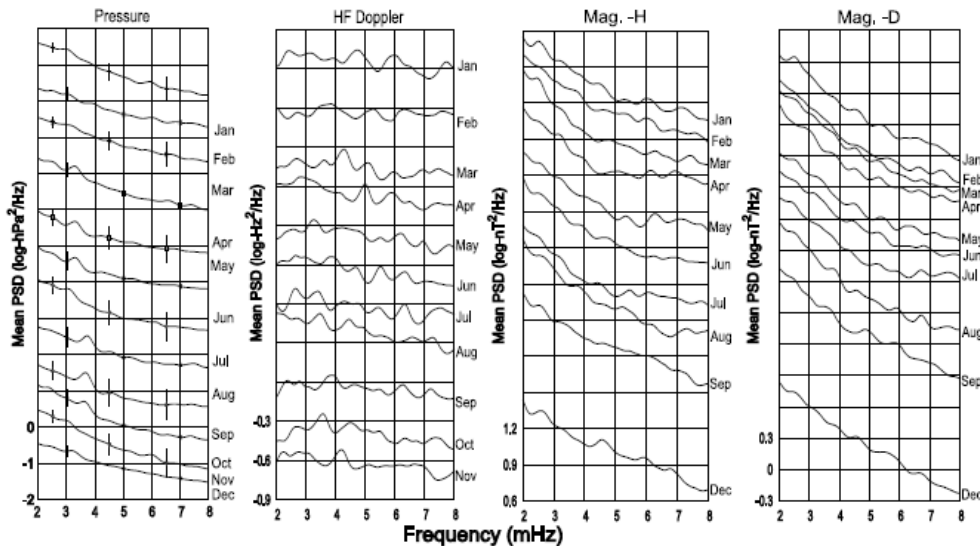


Figure 4: Mean PSDs in logarithmic scale in 2007. Pressure perturbations at Shigaraki, HF Doppler shifts at Oarai and geomagnetic variations of H and D components at Aso (from left to right). To avoid overlapping lines, PSD for each month is shifted from the next month by 1 for pressure, 0.3 for HFD, 0.3 for H, and 0.3 for D. The data of HFD in December and of magnetic components in September and October are missing. Error bars for pressure show standard error.

2.1.3 Mean coherencies over 12 months

Mean coherencies between pressure and HF Doppler, and pressure and magnetic components were calculated (Fig. 5). The Yule-Walker AR method was used to calculate coherencies. Data lengths, “Lag” of the AR model, and the average terms were the same as those of the PSDs. At 4.5 mHz, coherencies were a little higher in some months. The coherencies in the case of geomagnetic ap index ≤ 9 were used to decrease the effects of ionospheric disturbance and geomagnetic pulsations caused by magnetospheric plasma processes.

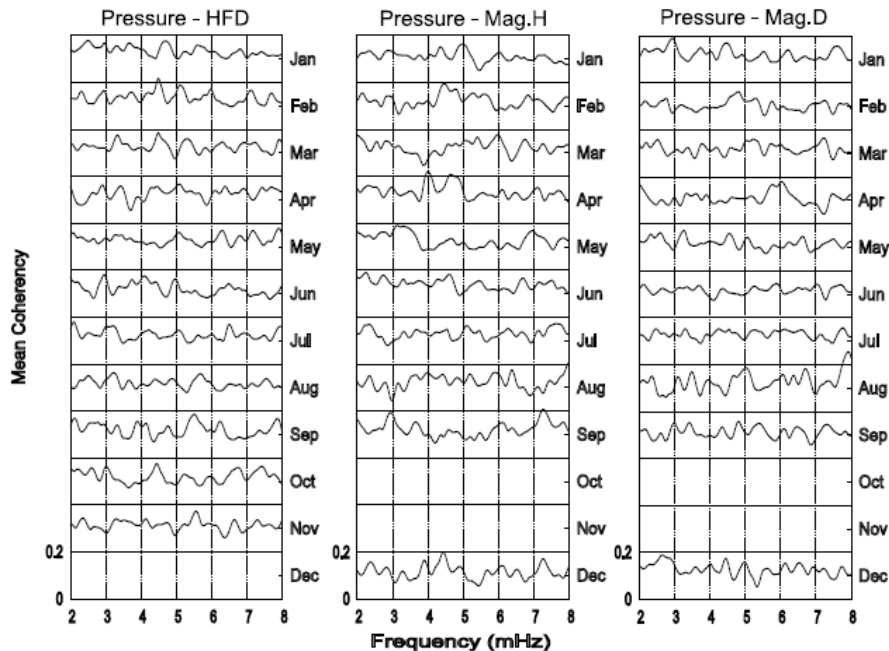


Figure 5: Mean coherencies in 2007. The left panel shows those between pressure and HF Doppler, the center panel shows those between pressure and magnetic H component, and the right panel shows those between pressure and magnetic D component. To avoid overlapping lines, coherency for each month is shifted from the next month by 0.2. The data of HFD in December and of magnetic components in September and October are missing.

3 DISCUSSION

The peaks of PSDs of pressure perturbation and HFD between 3 and 4 mHz, as shown in the figures of diurnal variations and in the monthly mean PSDs in Fig. 4, correspond to the theoretically expected resonance mode of $n = 1$ or 2 in the section 1.2.1. This result strongly suggests that acoustic resonance occurs.

There are three possible explanations for why the peaks of the pressure perturbations are clearer in April to October.

One explanation is that the pressure perturbations are more clearly observed because of a higher S/N ratio in this period; that is, the local turbulence is weak in this period at Shigaraki station. The second one is that the sources of acoustic waves are strong because of typhoons. The last one is that the temperature profile of the atmosphere is different at different seasons and acoustic resonance occurs more frequently in this period. The variation of the frequencies of the peaks with the months (Fig. 4) shows the variation of the temperature profile and the reflection heights of infrasounds with the months.

The peaks of HFD between 4 and 5 mHz shown in Fig. 4 correspond to the theoretically expected resonance mode of $n = 3$ or 4 in the previous section 1.2.1. Peaks around this frequency are also seen in the magnetic D component shown in Fig. 4, although this is not so clear. Moreover, the coherencies between pressure and HFD, pressure and magnetic H, and pressure and the magnetic D component also have peaks around this frequency (Fig. 5).

Peaks around 6 mHz for the magnetic H component might come from magnetospheric phenomena because resonance cannot occur at this frequency.

4 CONCLUSION

PSDs of pressure perturbations, ionospheric disturbances, and geomagnetic variations were calculated and averaged for each month. Peaks appeared at the theoretically expected resonance frequencies in the pressure and HF Doppler data. This shows that acoustic resonance exists and occurs frequently. The frequency varies with the seasons, probably because the vertical temperature profile of the atmosphere varies with the seasons and the reflection heights of infrasounds also vary.

Coherencies between pressure perturbations and ionospheric disturbances, and pressure and geomagnetic variations were also calculated and averaged for each month. Small peaks at the resonance frequencies in PSDs of geomagnetic variations and in the coherencies may show that geomagnetic variations are caused by acoustic resonance.

5 ACKNOWLEDGEMENTS

We thank Arai Nobuo, Murayama Takahiko, and Yamamoto Masayuki for providing useful information about barometric observations and Kobayashi Naoki, Nishida Kiwamu, and Yamamoto Ryozauro for useful observational and theoretical information. We also thank Tomizawa Ichiro and Ogawa Toru for helpful discussions about the HF Doppler method. The observations at Shigaraki were supported by the Shigaraki MU radar observatory; we thank the staff there for their help.

This study was partially supported by Grant-in-Aid 19654073 and the fund for the 21st Century COE Program (Kyoto University, G3). The HF Doppler data was provided by Sugadaira Space Radio Observatory, University of Electro-Communication.

6 REFERENCES

- Artru, J., Farges, T. and Lognonne, P. (2004), Acoustic waves generated from seismic surface waves: propagation properties determined from Doppler sounding observations and normal-mode modeling, *Geophys. J. Int.*, *158*, 1067–1077.
- Davies, K. and Jones, J. E. (1971), Ionospheric disturbances in the F2 region associated with severe thunderstorms, *J. Atmos. Sci.*, *28*, 254–262.
- Hedin, A. E. (1991), Extension of the MSIS thermospheric model into the middle and lower atmosphere, *J. Geophys.*

Res., 96, 1159.

Hino, M. (1977), The spectral analysis (in Japanese), *Asakura Publishing Co., Ltd.*, 221.

Iyemori, T. et al. (2005), Geomagnetic pulsations caused by the Sumatra earthquake on December 26, 2004, *Geophys. Res. Lett.*, 32, L20807, doi:10.1029/2005GL024083.

Jones, R. M. and Georges, T. M. (1976), Infrasound from convective storms. III. Propagation to the ionosphere, *J. Atmos. Sci.*, 59(4), 765–779.

Kanamori, H., Mori, J. and Harkrinder, H. G. (1994), Excitation of atmospheric oscillations by volcanic eruptions, *J. Geophys. Res.*, 99, B11, 21947–21961.

Kobayashi, N. (2007), A new method to calculate normal modes, *Geophys. J. Int.*, 168, 315–331.

Labitzke, K., Barnett, J. J. and Edwards, B., *Handbook MAP 16, SCOSTEP*, University of Illinois, Urbana, 1985.

Lognonne, P., Clevede, E. and Kanamori, H. (1998), Computation of seismograms and atmospheric oscillations by normal-mode summation for a spherical earth model with realistic atmosphere, *Geophys. J. Int.*, 135, 388–406.

Nishida, K., Kobayashi, N. and Fukao, Y. (2000), Resonant Oscillations Between the Solid Earth and the Atmosphere *Science*, 287, 2244–2246.

Nishida, K. (2000), Earth's background free oscillations, Ph.D. thesis, University of Tokyo.

Prasad, S. S., Schneck, L. J. and Davies, K. (1975), Ionospheric disturbances by severe tropospheric weather storms, *J. Atmos. Sci.*, 37, 1357–1363.

Shinagawa, H., Iyemori, T., Saito, S. and Murayama, T. (2007), A numerical simulation of ionospheric and atmospheric variations associated with the Sumatra earthquake on December 26, 2004, *Earth Planets Space*, 59, 1015–1026.

Tahira, M. (1995), Acoustic resonance of the atmosphere at 3.7 mHz, *J. Atmos. Sci.*, 52, 2670–2674.